Cluster Growth Reactions: Structures and Bonding of Metal-Rich Metallaheteroboranes Containing Heavier Chalcogen Elements

Chandan Nandi, Arindam Roy, Ketaki Kar, Marie Cordier, Sundargopal Ghosh

Cluster Growth Reactions: Structures and Bonding of Metal-Rich Metallaheteroboranes Containing Heavier Chalcogen Elements

Chandan Nandi,[a] Arindam Roy,[a] Ketaki Kar,[a] Marie Cordier,[b] and Sundargopal Ghosh[a]*

[a] Department of Chemistry, Indian Institute of Technology Madras, Chennai 600036, India

[b] Univ Rennes, CNRS, Institut des Sciences Chimiques de Rennes, UMR 6226, F-35000 Rennes, France

KEYWORDS: cobalt, decaborane, metallaheteroboranes, chalcogen, boron

ABSTRACT

In an effort to synthesize cobalt-rich metallaheteroboranes from decaborane(14) analogs, we have studied the reaction of 10-vertex *nido*-[(Cp*Co)$_2$B$_6$H$_6$E$_2$] (Cp* = η^5-C$_5$Me$_5$, **1**: E = Se and **2**: E = Te) with [Co$_2$(CO)$_8$] under thermolytic conditions. All these reactions yielded face-fused clusters, [(Cp*Co)$_2$B$_6$H$_6$E$_2${Co(CO)}(μ-CO){Co$_3$(CO)$_6$}] (**3**: E = Se and **4**: E = Te). Further, when clusters **3** and **4** were treated with [Co$_2$(CO)$_8$], they underwent further cluster build-up reactions leading to the formation of 16-vertex doubly-face-fused clusters [(Cp*Co)$_2$B$_6$H$_6$E$_2${Co$_2$(CO)$_2$}(μ-CO)$_2${Co$_4$(CO)$_8$}] (**5**: E = Se and **6**: E = Te). Cobaltaheteroboranes **3** and **4** comprise one icosahedron {Co$_4$B$_6$E$_2$} and one square pyramidal {Co$_3$B$_2$} moiety, whereas **5** and **6** are made with one icosahedron {Co$_4$B$_6$E$_2$} and two square pyramidal {Co$_3$B$_2$} cores. In an attempt to generate heterometallic metal-rich clusters, we have explored the reactivity of decaborane(14) analog *nido*-[(Cp*Co)$_2$B$_7$TeH$_9$] (**7**) with [Ru$_3$(CO)$_{12}$] at 80 °C, which afforded face-fused 13-vertex cluster [(Cp*Co)$_2$B$_7$H$_7$Te{Ru$_3$(CO)$_8$}] (**8**). Cluster **8** is a rare example of a metal-rich metallaheteroborane in which one icosahedron {Co$_2$Ru$_2$B$_7$Te} and a tetrahedron {Ru$_2$B$_2$} units are fused through a common {RuB$_2$} triangular face. Further, the treatment of *nido*-[(Cp*Co)$_2$B$_6$S$_2$H$_4$(CH$_2$S$_2$)] (**9**) with [Fe$_2$(CO)$_9$] afforded 11-vertex *nido*-[(Cp*Co)$_2$B$_6$S$_2$H$_4$(CH$_2$S$_2$){Fe(CO)$_3$}] (**10**). The core structure of **10** is similar to that of [C$_2$B$_9$H$_{11}$]$^{2-}$ with a 5-membered pentahapto coordinating face. All the synthesized metal-rich metallaheteroboranes have been characterized by multinuclear NMR spectroscopy, IR spectroscopy, ESI-mass, and structurally solved by single-crystal X-ray diffraction analysis. Furthermore, theoretical investigations gave insight into the bonding of such higher-nuclearity clusters containing heavier chalcogen atoms.

INTRODUCTION

Due to the presence of three valence electrons, boron is electron deficient and forms a covalently bonded three-dimensional network producing unusual structures both with the main group and transition metal elements.[1,2] Polyhedral boranes and their derivatives containing heteroatoms, such as carboranes, metallacarboranes, metallaboranes, and metallaheterobranes, with different organic moieties have shown significant influence in many areas of organic and inorganic chemistry,[3-6] for example, as catalysts, nanomaterials, polymers, ceramics and in BNCT (boron–neutron–capture–therapy).[4a,7] Apart from their applications, polyhedral boranes as well as their metal and heteroatom incorporated derivatives have shown a wide range of unusual synthetic and structural chemistry.[5a] Over the last fifty years, many main group pioneers, such as Lipscomb,[1a] Grimes,[3a] Fehlner,[4c,5a] Kennedy,[5b] Shore,[5c] Hawthorne,[7] Welch,[8] Xie,[9] and us[10] have reported various boron, carbon, chalcogen and transition metal-enriched single-cage as well as condensed polyhedral clusters. However, syntheses of these large polyhedra from small building block units are typically uncontrolled and mechanistically undefined.[11] The progress in this area was further enhanced by the development of both electron counting rules[12] and isolobal principle[13] that provided the groundwork for understanding the structural relationships between different clusters and their bonding motifs.

Numerous complementary approaches to the expansion of cluster networks are available especially to build higher vertices metallaborane and metallaheteroborane clusters. For example, (i) condensation reactions by using monoborane reagents, such as [BH_3·THF] or [$LiBH_4$·THF],[10a,b] (ii) insertion or fragmentation by using metal carbonyl fragments or borane,[6] and (iii) the intercluster fusion of smaller to higher clusters such as tetrahedral, octahedral, and trigonal-prismatic, square antiprismatic, or icosahedral fragments with one, two or more atoms

held in common between the subclusters.[10e,14] Nonetheless, the single-cage clusters rich with boron, metal, and other main group elements are rare.[11] As a result, finding viable synthetic methods for such higher nuclearity clusters became of interest.

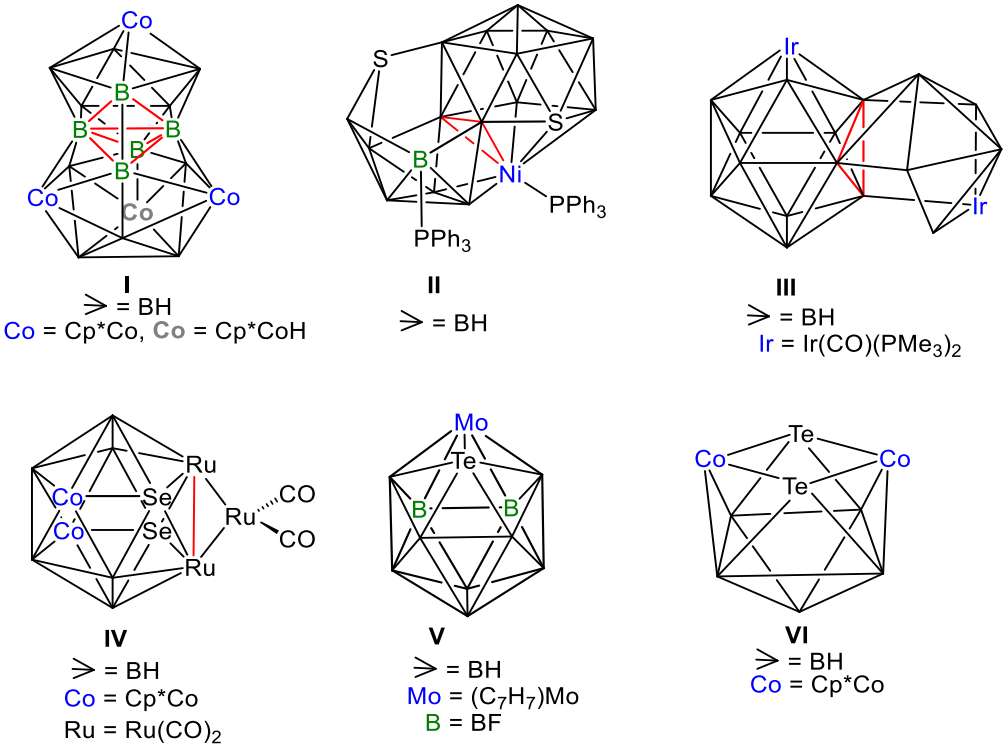

Chart 1. Polyhedral and macropolyhedral metallaboranes and metallaheteroboranes.

In our continuing efforts to synthesize metallaboranes and metallaheteroboranes, we have recently synthesized and characterized a 19-vertex face-fused cluster *closo*-[$(Cp^*Co)_3B_{15}H_{10}${Cp*CoH}] (**I**).[14] As shown in Chart 1, **I** is composed of one icosahedron {Co_3B_9}, one tetrahedral {B_4} and one bicapped square-antiprismatic {CoB_9} core, which are fused by one {B_3} triangular and one {B_4} butterfly face.[14] Kennedy and co-workers have reported a 19-vertex nickeladithiaborane [$(PPh_3)NiS_2B_{16}H_{12}(PPh_3)$] (**II**) comprising a 9-vertex *nido*-{NiB_8} and one 12-vertex *closo*-{$NiSB_{10}$}, which are fused by a triangular {NiB_2} face.[15] Subsequently,

the same group has synthesized an 18-vertex macropolyhedral diiridaborane(**III**), composed of one 8-vertex *nido*-{IrB_7} and one 12-vertex *closo*-{IrB_{11}}, fused by two common boron atoms.[16] Although several macropolyhedral metallaboranes and metallathiaboranes are known in the literature, single-cage, and condensed clusters containing heavier chalcogen atoms, especially selenium and tellurium are limited. Recently, we have isolated a fused cluster, 13-vertex *closo*-[$(Cp^*Co)_2B_6H_6Se_2\{(CO)_8Ru_3\}$] (**IV**), composed of one {$Co_2Ru_2B_6Se_2$} icosahedron and a triangle {Ru_3}, fused through {Ru_2} edge.[6b] Spalding and co-workers have isolated a 12-vetex B-fluorinated *closo*-[$(\eta^7\text{-}C_7H_7)F_2MoTeB_{10}H_8$] (**V**), which is the first example of a paramagnetic transition element complex having Te atom in the cluster core.[17] Further, in the quest for polyhedral clusters comprising heavier chalcogen atoms, we have recently isolated a 9-vertex *nido*-[$(Cp^*Co)_2B_5H_5Te_2$] (**VI**).[18] As a result, isolation of higher vertices clusters comprising heavier chalcogen atoms following a cohesive synthetic route became appealing. In this paper, we have re-examined the chemistry of decaborane(14) analogs with different metal carbonyls, such as [$Co_2(CO)_8$], [$Ru_3(CO)_{12}$], and [$Fe_2(CO)_9$] that afforded higher nuclearity metallaheteroborane clusters with unusual geometries. Herein, we discussed the syntheses, structure, and bonding of unusual 14- and 16-vertex face-fused clusters comprising group 16 heavier elements.

RESULTS AND DISCUSSION

Reactivity of *nido*-1 and *nido*-2 with [$Co_2(CO)_8$]. The various interesting structural patterns, shown in Chart 1, motivated us to synthesize higher nuclearity metallaheteroboranes comprising heavier chalcogen atoms. Cluster expansion using transition metal carbonyls is a notable way to form higher-vertex clusters. Therefore, the reactivities of *nido*-**1** and *nido*-**2** with [$Co_2(CO)_8$] have been explored. As shown in Scheme 1, reactions of *nido*-**1** and **2** with [$Co_2(CO)_8$] at 80 °C

led to the formation of **3** and **4**, respectively. Clusters **3** and **4** were synthesized as brown solids in 18% (R_f = 0.356) and 24% (R_f = 0.363) yields, respectively, and characterized by multinuclear NMR spectroscopy, mass spectrometry, and IR spectroscopy. In the ^{1}H NMR, both **3** and **4** show one chemical shift at δ = 1.77 and 1.86 ppm, respectively, corresponding to single Cp* environment. Furthermore, the $^{13}C\{^{1}H\}$ NMR validate the existence of one Cp* environment for **3** and **4**. The ^{1}H NMR spectra display one broad upfield peak at δ = -4.42 and -4.86 ppm for **3** and **4**, respectively, due to Co-*H*-B protons. To establish the nature and connectivity of protons, the $^{1}H\{^{11}B\}-^{11}B\{^{1}H\}$ HSQC NMR experiments of **3** and **4** were performed that established a correlation between the bridging hydrogens and the boron resonance observed at δ = 24.5 and 27.3 ppm, respectively (Figures 1, S12 and S20). In addition, the IR spectra of **3** and **4** display distinctive peaks for CO and BH_t. The $^{11}B\{^{1}H\}$ NMR spectrum displays four resonances at δ = 35.6, 30.4, 24.5, and 2.6 ppm in ~1:1:2:2 intensity ratio for **3**; whereas **4** shows four peaks at δ = 38.9, 27.3, 26.6, and 8.1 ppm in ~1:2:1:2 intensity ratio. The ESI-MS spectra show isotopic patterns $[M+Na]^+$ at *m/z* 1100.7235 and 1196.6965 for **3** and **4**, respectively, that confirm the cluster frameworks with different chalcogen atoms [**3**:Se and **4**:Te]. Finally, the single-crystal X-ray diffraction analyses were performed to determine the solid-state structures of **3** and **4**.

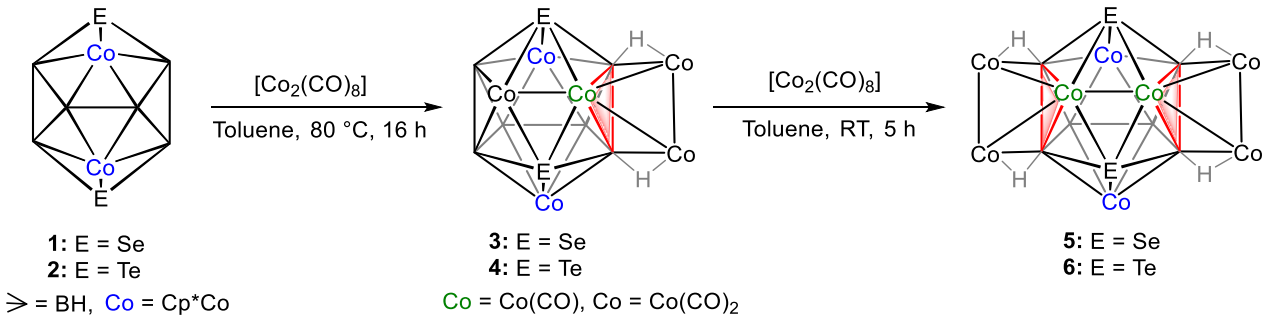

Scheme 1. Syntheses of face-fused and doubly-face-fused metallaheteroboranes **3**-**6**.

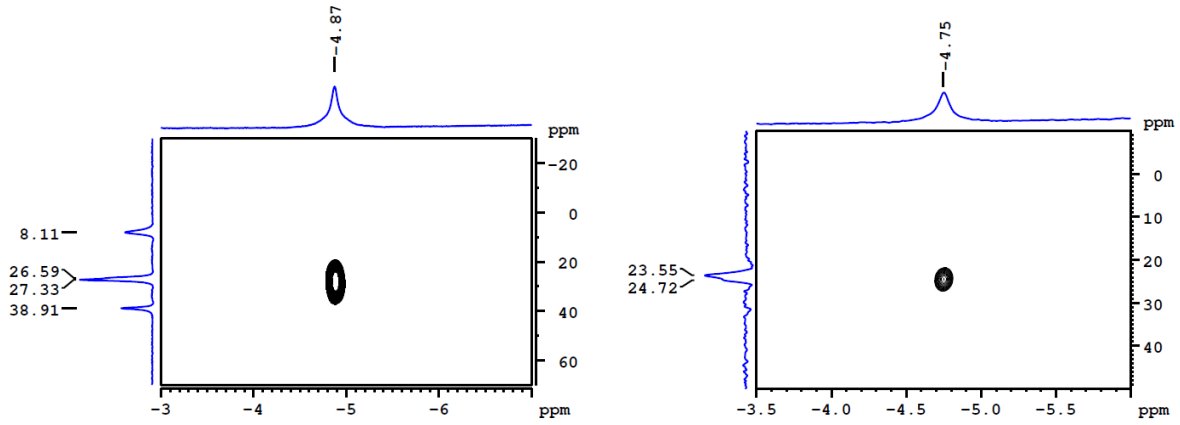

Figure 1. $^{1}H\{^{11}B\}$-$^{11}B\{^{1}H\}$ HSQC NMR spectra of **4** (left) and **5** (right).

Single crystals of these clusters appropriate for XRD analyses were grown at −5 °C from the solution of CH_2Cl_2-hexane (30:70). The X-ray structures of both **3** and **4**, shown in Figure 2, correspond to 14-vertex face-fused $[(Cp^*Co)_2B_6H_6E_2\{Co(CO)\}(\mu\text{-}CO)\{Co_3(CO)_6\}]$ (**3**: E = Se; **4**: E = Te) clusters that contain six cobalt, six boron, and two chalcogen atoms. The framework geometries of both **3** and **4** comprise a 12-vertex icosahedron $\{Co_4B_6E_2\}$ and five vertex $\{Co_3B_2\}$ *nido*-square pyramid unit. One common triangular face, Co-B-B is shared by both the polyhedra. The average bond distances B-B (1.77 Å) and Co-B (2.16 Å) of **3** and **4** are comparable with reported cobaltaboranes.[14] Considering the Mingos fusion formalism,[12b] the cluster valence electrons (CVE) for **3** and **4** are computed by the addition of valence electrons of icosahedron, [14×4 (Co) + 4×6 (B) + 4×2 (Se/Te) + 2 = 90] and square pyramid [14×3 (Co) + 4×2 (B) + 4 = 54] followed by subtraction of the common triangle [16×1 (Co) + 6×2 (B) = 28] that provided a total of 116 cluster valance electrons. This is being satisfied from the available cluster valence electrons for **3** and **4** [(6×9 (Co) + 2×5 (Cp*) + 6×3 (B) + 6×1 (H) + 8×2 (CO) + 2×6 (Se/Te) = 116].

In order to synthesize metal-rich metallaheteroboranes, we were curious to explore a similar kind of reactivity with a different type of decaborane(14) analogs, and hence, we treated $[(Cp^*Co)_2B_7TeH_9]$, *nido*-**7**[19] with $[Co_2(CO)_8]$. Unfortunately, the reactivity of *nido*-**7** with $[Co_2(CO)_8]$ did not generate mono face-fused clusters. This may be due to the presence of a single chalcogen atom in the decaborane(14) core that could not offer the necessary coordination environment as observed in the case of *nido*-**1** and **2**.

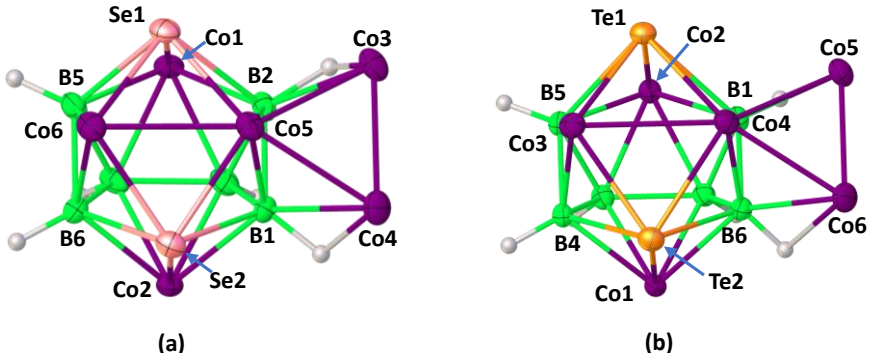

Figure 2. Solid-state structures of **3**(a) and **4**(b). Thermal ellipsoids are set at the 40% probability level. Note that, for clarity Cp* (attached to Co1 and Co2) and the carbonyl groups (attached to Co3, Co4, Co5, and Co6) are omitted. Selected bond lengths (Å) and angles (°). **3**: B5-B6 1.784(12), B6-Co6 2.216(9), B1-Co2 2.128(8), B1-Co5 2.135(9), B1-Se2 2.249(8), B2-Se1 2.282(8), B5-Se1 2.160(8); B2-B1-Co2 117.4(5), Co2-B1-Co5 122.4(4), Co3-Co5-Co4 58.63(4); **4**: B1-B6 1.741(5), B1-Co2 2.139(4), B1-Co4 2.126(4), B1-Te1 2.439(4), B4-Te2 2.414(4), B4-Co1 2.150(4), Co5-Co6 2.4319(7), Co4-Te1 2.5058(5), Co3-Co4 2.7470(7); B6-B1-Co2 118.9(2), Te2-Co3-Te1 107.553(19).

To provide some insight into the electronic structures and bonding relationship of such high nuclearity metallaheteroborane clusters, the DFT calculations using the Gaussian 16 program with a B3LYP/def2-TZVP level of theory for **3′** and **4′** (Cp analogs of **3** and **4**) have been carried out (see computational details in the supporting information (SI)). The calculated bond distances and the ^{11}B NMR resonances for **3′** and **4′** are in good accordance with the structural and

experimental parameters (Tables S1 and S2). The frontier MO analyses clearly show a higher HOMO-LUMO gap in **3′** (~2.577 eV) as compared to **4′** (~2.500 eV). This may be due to the presence of different chalcogen atoms in their cluster framework (Table S6). As shown in Figure 3, the HOMOs of **3′** and **4′** are predominantly concentrated on Co (d-orbitals), whereas their LUMOs display mainly antibonding interaction along the Co-Co bond in the icosahedron core. On the other hand, the HOMO-1 and HOMO-2 of **3′** and **4′**, respectively, show notable bonding interaction with three Co-centers at one side of the icosahedron. In addition, the antibonding interaction along the Co-E (E = Se, Te) bond on other side of the icosahedron resulted in bulging out of the metal d-orbital outwards. As a result, one might assume further interaction with metal carbonyl fragments leading to additional cluster growth reactions. The donating nature can also be observed from the natural charge and natural valence population calculations, achieved from NBO analyses of **3′** and **4′** (Table S4).

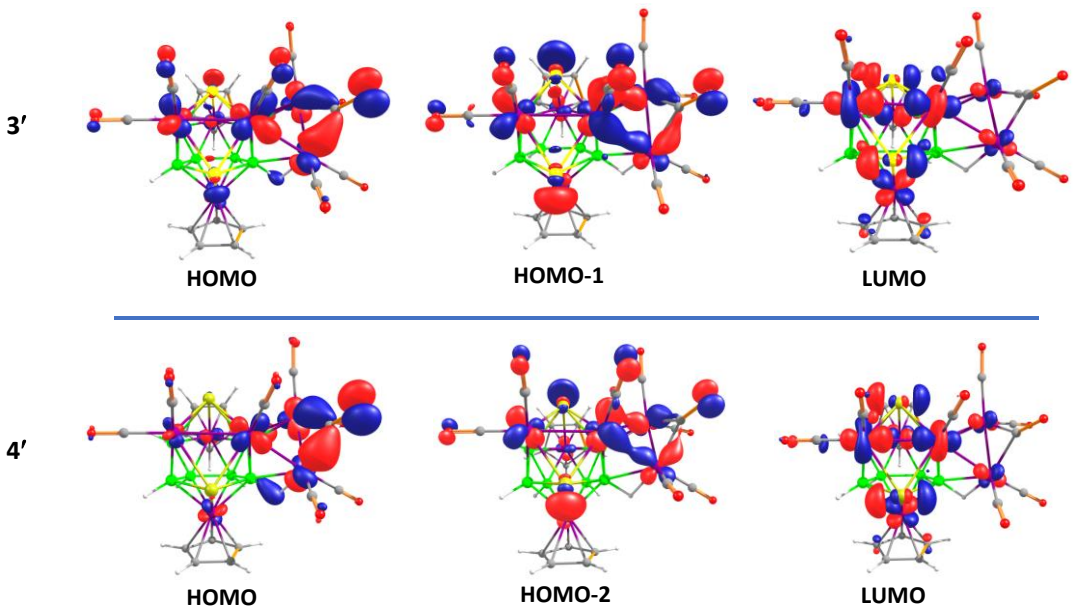

Figure 3. Selected molecular orbitals of **3′** and **4′**. Isosurfaces are plotted at an isovalue of ±0.04 $(e/bohr^3)^{1/2}$.

Reactivity of face-fused clusters 3 and 4 with [$Co_2(CO)_8$]. Theoretical calculations on clusters **3′** and **4′** suggested the further possibility of cluster expansion if treated with transition metal carbonyls. As a result, we have further explored the reactivity of **3** and **4** with [$Co_2(CO)_8$] aiming sequential cluster expansion reaction. As shown in Scheme 1, room temperature reactions of **3** and **4** with 2 equivalents of [$Co_2(CO)_8$] yielded brown solids **5** (16% yield, R_f = 0.214) and **6** (21% yield, R_f = 0.227), respectively. The ^{1}H chemical shifts at δ = 1.82 and 1.89 ppm for **5** and **6**, respectively, correspond to Cp* protons, which have been further verified by $^{13}C\{^1H\}$ NMR. In addition, the ^{1}H NMR spectra of **5** and **6** display one upfield resonance at δ = -4.75 and -5.05 ppm, respectively, due to the presence of Co-*H*-B proton(s). Further, the $^1H\{^{11}B\}-^{11}B\{^1H\}$ HSQC NMR experiments of **5** and **6** were performed that established a correlation between the bridging hydrogens and the $^{11}B\{^1H\}$ resonance observed at δ = 23.5 and 27.2 ppm, respectively (Figures 1, S28, and S35). In addition, the IR spectra of **5** and **6** show stretching frequencies for BH_t and CO groups. The $^{11}B\{^1H\}$ NMR spectrum displays peaks at δ = 24.7 and 23.5 ppm for **5**, whereas for **6** shows one resonance at δ = 27.2 ppm, which may be due to the accidental overlap of the two peaks. This has further supported by theoretical ^{11}B NMR chemical shift values that show minor differences (Table S1). The ESI-MS spectra display isotopic patterns at *m/z* 1308.5886 $[M+H]^+$ and 1405.5727 $[M+H]^+$ for **5** and **6**, respectively. Although all the spectroscopic assignments suggest similar structures for **5** and **6**, the X-ray analyses provided their core structures.

The X-ray quality crystals suitable for **5** and **6** were obtained at −5 °C by slow evaporation of a CH_2Cl_2-hexane solution. As shown in Figure 4, the solid-state X-ray structures of **5** and **6** correspond to 16-vertex doubly-face-fused clusters [$(Cp^*Co)_2B_6H_6E_2\{Co_2(CO)_2\}(\mu\text{-}CO)_2\{Co_4(CO)_8\}$] (**5**: E = Se; **6**: E = Te) that contain eight cobalt, six boron and two chalcogen atoms. Two

common triangular faces are involved for the fusion of three polyhedra, for example, 12-vertex icosahedron $\{Co_4B_6E_2\}$ and two 5-vertex *nido*-square pyramid $\{Co_3B_2\}$ units. The average Co-E [2.33 Å (Se), 2.47 Å (Te)], Co-B (2.16 Å), and B-B (1.77 Å) bond distances of clusters **5** and **6** are within the range of reported cobaltachalcogenaboranes.[6b] The cluster fusions of **5** and **6** are fascinating, in which three polyhedra are involved to form 16-vertex macropolyhedra. Ignoring the crystallographic limitations, the core geometries of **5** and **6** have C_{2v} symmetry, where the C_2 axis crosses through the middle of of B-B and Co-Co bonds. Note that, the ^{1}H chemical shifts for Co-*H*-B hydrogens for **3**-**6** are significantly downfield shifted than typically observed for M-*H*-B

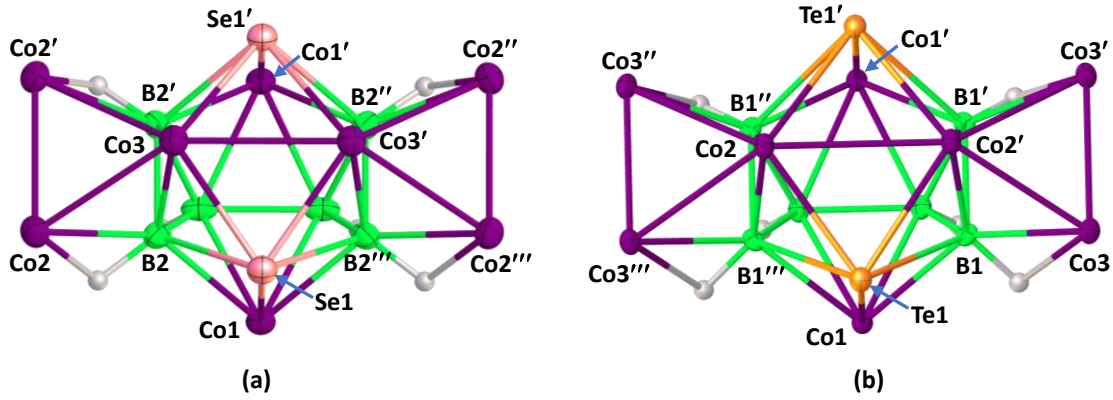

Figure 4. Molecular structures of **5**(a) and **6**(b). (′, ″, ‴,) are used to indicate symmetry-generated atoms. Note that, Cp* ligands are attached to Co1, Co1′ (for **5** and **6**); and carbonyl ligands attached to Co2, Co2′, Co2″, Co2‴, Co3, Co3′ (for **5**) and Co2, Co2′, Co3, Co3′, Co3″, Co3‴ (for **6**) are omitted for clarity. Thermal ellipsoids are set at the 40% probability level. Selected bond lengths (Å) and angles (°). **5**: Co1-B2 2.118(9), Co1-Se1 2.3177(18), Co2-Co3 2.4896(17), Co3-B2 2.117(10), Co3-Co3′ 2.651(3), Se1-B2 2.242(9), B2-B2′ 1.73(2); B2′-Co1′-B2″ 94.2(5), B2-Co1-Se1 60.5(3), B2-Co2-Co2′ 81.0(3), B2-Co2-Co3 52.9(2), Co2-Co3-Co2′ 58.33(6); **6**: B1-Te1 2.444(5), Co2-Te1 2.4646(6), Te1-Co1 2.4661(9), Co1-B1 2.141(5), Co2-B1‴ 2.137(5), Co2-Co3″ 2.4901(9), Co2-Co2′ 2.7938(15); B1-Te1-B1‴ 81.7(2), B1-Te1-Co2′ 51.61(11), Co2-Te1-Co2′ 69.05(3), B1-Te1-Co1 51.69(11), Co2-Te1-Co1 99.28(3), B1-Co1-Te1 63.63(12).

hydrogens. They are comparable to B-*H*-B hydrogens.[14] Theoretical insight into the bonding situation of **3′**-**6′** showed that the Wiberg bond indices (WBIs) of the B-H_b interaction are significantly higher than those of Co-H_b bond and in the range of terminal B-H bond (Table S3). In addition, the bond occupancy of the bridged B-H_b (eg. 1.720 for **4′**) is further nearer to the terminal B-H bond (eg. 1.943 for **4′**) that illustrates stronger B-H_b interaction as compared to Co-H_b interaction in Co-*H*-B.

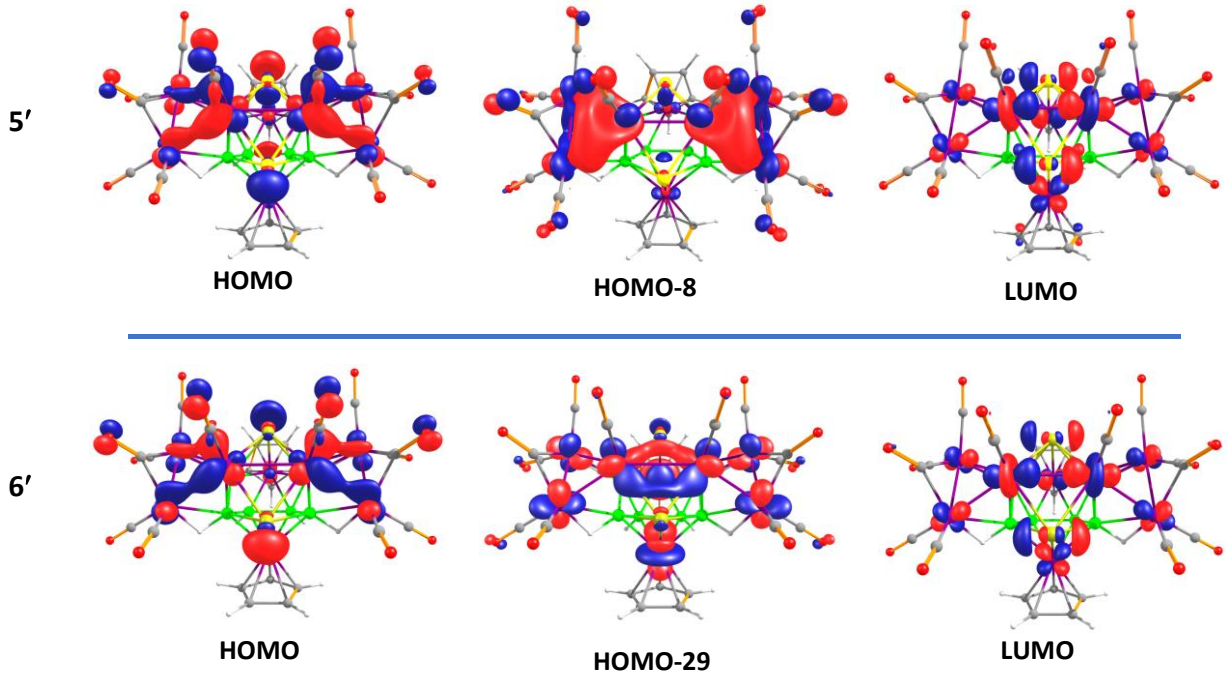

Figure 5. Selected molecular orbitals of **5′** and **6′**. Isosurfaces are plotted at an isovalue of ±0.04 $(e/bohr^3)^{1/2}$.

The face-fused clusters of **5** and **6** contain 142 cluster valence electrons [(8×9 (Co) + 2×5 (Cp*) + 6×3 (B) + 6×1 (H) + 12×2 (CO) + 2×6 (Se/Te) = 142]. According to Mingo's approach,[12b] the cluster valence electrons (CVE) for **5** and **6** are also 142. For example, [(one icosahedron + two square pyramids) minus two triangles; {14×4 (Co) + 4×6 (B) + 4×2(Se/Te) +

2} + {2(14×3 (Co) + 4×2 (B) + 4)} – {2(16×1 (Co) + 6×2 (B)} = 142]. Hence, both clusters obey Mingos fusion formalism.

The HOMOs of both **5′** and **6′** (Cp analogs of **5** and **6**) show significant bonding interaction between Co-centers while the LUMOs are mainly concentrated on the cobalt d-orbitals and (Se/Te) p-orbitals with antibonding interaction along the metal-metal bond same as observed in **3′** and **4′** (see computational details in SI). Further, the HOMO-8 of **5′** shows trimetallic-bonding interaction between the cobalt centers in which one of the Co atoms directly involved in the fusion of cluster and the HOMO-29 of **6′** represents an extended orbital overlap of cobalt d-orbitals and (Se/Te) p-orbitals (Figure 5). Topology analyses using the QTAIM approach and Wiberg bond indices also support the overall bonding scenario (Tables S2 and S5).

Reactivity of *nido*-7 with $[Ru_3(CO)_{12}]$. Although *nido*-**7** does not participate in cluster growth reaction with $[Co_2(CO)_8]$, we were interested in checking the same reaction with $[Ru_3(CO)_{12}]$. As a result, we have studied the chemistry of *nido*-**7** with $[Ru_3(CO)_{12}]$. The reactivity of *nido*-**7** with $[Ru_3(CO)_{12}]$ at 80 °C yielded **8** as violet solid (11% yield, R_f = 0.342) (Scheme 2). The ^{1}H NMR spectrum exhibit two different Cp* environments at δ = 1.76 and 1.63 ppm in ~1:1 ratio, which was also established by the $^{13}C\{^1H\}$ NMR spectrum. Cluster **8** shows one upfield resonance in the ^{1}H NMR spectrum at δ = -8.92 ppm, which is due to the presence of Ru-*H*-B proton(s). Further, the $^1H–^{11}B\{^1H\}$ HSQC NMR experiment of **8** was performed that established a correlation between the bridging hydrogens and the boron resonance observed at δ = 14.9 ppm (Figure S41). The $^{11}B\{^1H\}$ NMR spectrum of **8** shows peaks at δ = 50.0, 39.4, 35.8, 14.9, and 5.6 ppm with an intensity ratio of ~1:1:1:3:1. In addition, the infrared spectrum (IR) of **8** displays peaks for CO ligands and BH_t. The ESI-MS spectrum of **8** shows a isotopic patterns at *m/z* 1126.7909 $[M]^+$.

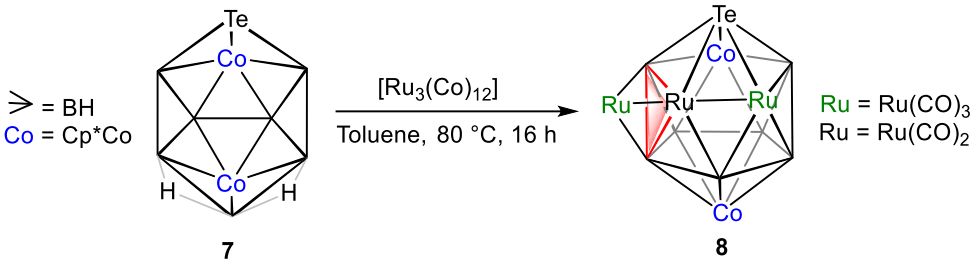

Scheme 2. Synthesis of metallaheteroboranes **8**.

Although the formation of a higher-nuclearity cluster is supported by all available spectroscopic and mass spectrometric data, it was difficult to predict the precise geometry until an X-ray analysis established the core structure and molecular formula of **8** as $[(Cp^*Co)_2B_7H_7Te\{Ru_3(CO)_8\}]$. The solid-state molecular structure of **8**, shown in Figure 6, displays a face-fused 13-vertex cluster consisting of 12-vertex icosahedron $\{Co_2Ru_2B_7Te\}$ and a tetrahedron $\{Ru_2B_2\}$ unit, in which one common triangular face {Ru-B-B} is shared for both the polyhedra. According to Mingos fusion formalism,[12b] the number of cluster valance electrons

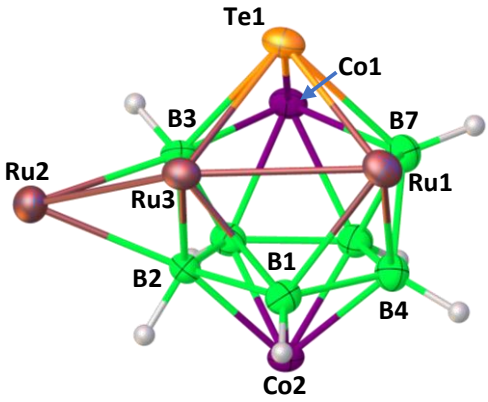

Figure 6. X-ray structure of **8**. Thermal ellipsoids are set at the 40% probability level. For clarity Cp* ligands attached to cobalt, carbonyl groups attached to ruthenium, and one CH_2Cl_2 molecule are omitted. Selected bond distances (Å) and angles (°): B3-Co1 2.103(7), Co1-B7 2.197(7), Co1-Te1 2.4692(9), Co2-B2 2.026(7), Ru1-Te1 2.6571(7), Ru1-B7 2.451(7), Ru1-Ru3 2.8175(7), Ru2-Ru3 2.7242(7), Ru3-Te1 2.6674(6), Te1-B3 2.397(7); B3-Co1-B7 94.2(3), B7-Co1-Te1 64.24(19).

(CVE) for **8** is computed by the addition of valance electrons of an icosahedron, [14×2 (Co) + 14×2 (Ru) + 4×7 (B) + 4×1 (Te) + 2 = 90] and a tetrahedron [15×2 (Ru) + 5×2 (B) = 40] followed by subtraction of common triangle [16×1 (Ru) 6×2 (B) = 28], which provided a total of 102 cluster valance electrons. This is being satisfied from the available cluster valance electrons for **8** [2×9 (Co) + 3×8 (Ru) + 2×5 (Cp*) + 7×3 (B) + 7×1 (H) + 8×2 (CO) + 1×6 (Te) = 102].

The HOMO–4 of **8′** (Cp analog of **8**) shows a significant overlap of the d_z^2 orbitals of Ru3 and Ru2, indicating notable bonding interaction between two Ru centers (Figure S55). Moreover, the Wiberg Bond Index (WBI) of 0.4084 between two Ru centers validates the Ru−Ru bonding interaction. Further, as shown in Figure 7, the HOMO-27 shows a three-center overlap of orbitals involving two Ru atoms and one Te atom extended along the icosahedron core. Laplacian electron density plot of **8′** also depict the above bonding picture (Figure 7).

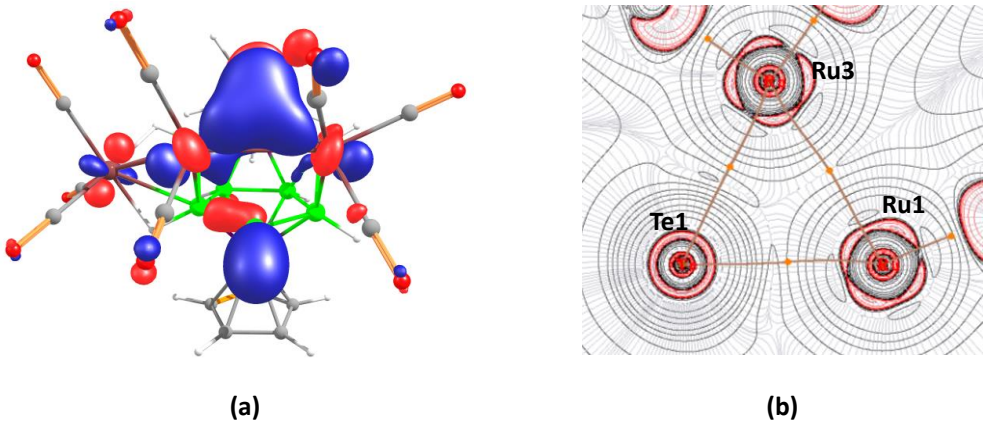

Figure 7. (a) Frontier molecular orbital (HOMO-27) of **8′**. (b) Laplacian electron density plots of **8′** of the plane Ru1−Te1−Ru3, where the charge depletion ($\nabla^2 \rho(r) > 0$) areas shown by dashed black lines, while solid red lines indicate areas of charge concentration ($\nabla^2 \rho(r) < 0$). Orange dots indicate BCPs (bond critical points).

Reactivity of *nido*-9 with $[Fe_2(CO)_9]$. Our earlier attempts for cluster build up reactions of *nido*-**1** with $[Fe_2(CO)_9]$ yielded 11-vertex *nido*-$[(Cp^*Co)_2B_6Se_2H_6\{Fe(CO)_3\}]$.[6b] The core geometry of

this 11-vertex cluster was uncommon and comparable to $[C_2B_9H_{11}]^{2-}$ with a distinct 5-membered open face comprising more polarized bonds. As a result, with an objective to close this central open 5-membered face, we have carried out reactions with various 2-electrons metal fragments. However, all our attempts to get 12-vertex icosahedral core failed. Recently, we have isolated a $\{CS_2\}$ supported decaborane(14) analog, $[(Cp^*Co)_2B_6S_2H_4(CH_2S_2)]$, *nido*-**9** having an open face.[19] Thus, with a similar objective, we have carried out the reaction of *nido*-**9** with the same set of reactants that afforded purple solid **10** (28% yield, R_f = 0.282) (Scheme 3). The $^{11}B\{^1H\}$ NMR spectrum displays resonances in ~2:2:1:1 intensity ratio at δ = 34.8, 30.7, 26.2, and 6.9 ppm for **10**. The ^1H NMR displays a peak at δ = 1.65 ppm, which confirms the presence of a single Cp* environment. Further, the ^1H and $^{13}C\{^1H\}$ NMR spectrum of **10** confirms the presence of the methylene group. In addition, the IR spectrum displays distinctive peaks for BH_t and CO ligands for **10**. The ESI-MS spectrum of **10** shows a peak at 739.0144 $[M]^+$ that corresponds to the molecular formula of $C_{24}H_{36}B_6Co_2FeO_3S_4$. Finally, the molecular structure of **10** was confirmed by X-ray diffraction analysis. As shown in Figure 8(a), the X-ray structure reveals a 11-vertex $[(Cp^*Co)_2B_6S_2H_4(CH_2S_2)Fe(CO)_3]$ heterometallic cluster having 26 skeletal electrons that follow Wade's rule: $[2\{Cp^*Co\} + 2\{\mu_3\text{-}S\} + 4\{BH\} + 1\{Fe(CO)_3\} + 1\{B_2CH_2S_2\}] = [2\times(2) + 2\times(4) + 4\times(2) + 1\times(2) + 1\times(4)] = 26]$.

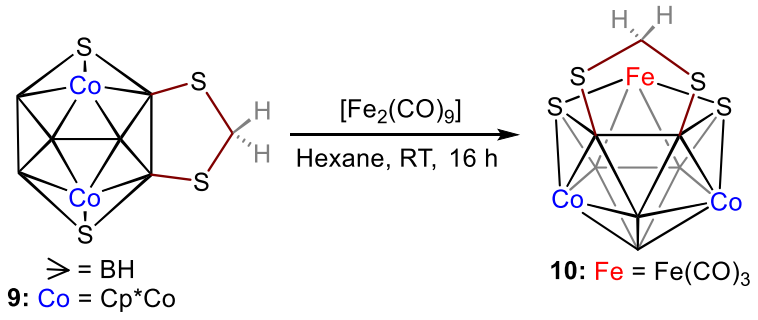

Scheme 3. Synthesis of metallaheteroborane **10**.

The HOMO of **10′** (Cp analog of **10**) shows significant bonding interactions between B and Co atoms along with the antibonding interactions between Co and S atoms of methanedithiolate (CH_2S_2) moiety (Figure S56). In addition, the HOMO-4 shows directed p-orbitals on S-atoms of the decaborane core that is inclined towards the pentagonal face (Figure 8(b)). Thus, one may assume that this molecule might show further cluster growth reaction if treated with two-electron metal or main group fragments. As a result, we have studied the reactions of *nido*-**10** with $[Co_2(CO)_8]$ both under room temperature and thermolytic conditions. However, the objective of getting *closo*-icosahedral from *nido*-**10** was not achieved. This may be due to the fact that $\{Fe(CO_3)\}$ and $\{CS_2\}$ bridged units in *nido*-**10** are oriented in such a fashion that prevents bonding interaction between the S-atom and additional metal carbonyl fragment.

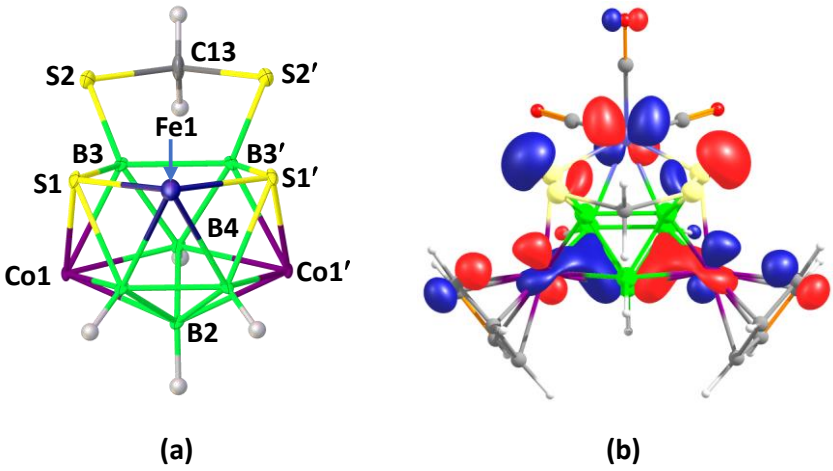

Figure 8. (a) Molecular structure of **10**. Thermal ellipsoids are set at the 40% probability level. Cp* ligands attached to cobalt, carbonyl ligands attached to iron, and one CH_2Cl_2 molecule are omitted for clarity. Selected bond distances (Å) and angles (°): Co1′-S1′ 2.2081(17), Co1-B3′ 2.072(7), Co1-B2 2.095(5), Fe1-S1 2.3033(18), S1-B3 1.867(7), B3-B3′ 1.857(13), S2-B3 1.856(7), S2-C13 1.817(6), B3-B4 1.799(10); B4-Co1-B1 87.7(3), B3-Co1-S1 51.6(2), B4-Co1′-S1′ 92.3(3), S1-Fe1-S1′ 92.78(9), S2′-B3′-S1′ 118.4(4), S2-C13-S2′ 111.6(5); (b) Frontier molecular orbital (HOMO-4) of **10′**.

CONCLUSION

In summary, the cluster expansion reactions of *nido*-[(Cp*Co)$_2$B$_6$H$_6$E$_2$] (**1**: E = Se and **2**: E = Te) by employing [Co$_2$(CO)$_8$] yielded 14-vertex face-fused clusters **3** and **4**. Further reaction of 14-vertex **3** and **4** with [Co$_2$(CO)$_8$] produced 16-vertex doubly-face-fused clusters **5** and **6**. In addition, a 13-vertex face-fused heterometallic metallaheteroborane **8** has been isolated and structurally characterized. The cluster fusion that generated 14 and 16-vertex fused clusters is rare. Also, the core geometry of **8** in which an icosahedron and a tetrahedron unit are fused through a common triangular face is unique in metallaborane cluster chemistry. Furthermore, the chemistry of {CS$_2$}-supported decaborane(14) analog *nido*-**9** with [Fe$_2$(CO)$_9$] was explored, which yielded 11-vertex *nido*-**10**. The 5-membered open face of *nido*-**10** is very similar to [C$_2$B$_9$H$_{11}$]$^{2-}$. Thus, the explorations to evaluate the scope for further cluster growth reactions of *nido*-**10** with small molecules and transition metal fragments are underway and we anticipate additional progress in the future.

Experimental Section

General Procedures and Instrumentation. All the syntheses were performed in an argon atmosphere using Schlenk line techniques. Under an argon atmosphere, dichloromethane, toluene, THF, and hexane were distilled using Na/benzophenone before use. All chemicals, such as [Co$_2$(CO)$_8$], [Ru$_3$(CO)$_{12}$], [Fe$_2$(CO)$_9$], were bought from Sigma Aldrich and used without purification. The starting materials *nido*-[(Cp*Co)$_2$B$_6$H$_6$E$_2$] (**1**: E = Se; **2**: E = Te),[6b] *nido*-[(Cp*Co)$_2$B$_7$TeH$_9$], **7**[19] and *nido*-[(Cp*Co)$_2$B$_6$S$_2$H$_4$(CH$_2$S$_2$)], **9**[19] were synthesized according to the literature procedures. All the clusters described here are reproducible. These reactions were carried out multiple times, which provided the same product distribution. Dialuminium-

supported TLC plates (MERCK TLC Plates) were used to separate the reaction mixtures. The 400 and 500 MHz Bruker FT-NMR spectrometers were used to record NMR spectra. Residual solvent carbon ($CDCl_3$, δ = 77.1 ppm) and protons ($CDCl_3$, δ = 7.26 ppm) were used as a reference for the $^{13}C\{^1H\}$ and ^1H NMR spectra, respectively. The inverse gated decoupling (zgig) and power gated (zgpr) pulse sequences, respectively, were used to get the $^{11}B\{^1H\}$ and the $^1H\{^{11}B\}$ spectra. A commercial Bruker spectrometer has access to all pulse sequences. The ESI-MS of the synthesized clusters were recorded using the 6545 Qtof LC/MS and Qtof Micro YA263 HRMS instruments. The IR spectra were obtained in CH_2Cl_2 solvent using JASCO FT/IR-1400 spectrometer.

Syntheses of metallaheteroboranes 3 and 4. In a flame-dried Schlenk tube, under an argon atmosphere, the yellow solution of *nido*-**1** (0.030 g, 0.048 mmol) in dry toluene (10 mL) was charged dropwise with a solution of $[Co_2(CO)_8]$ (0.096 mmol, 0.033 g) in 5 mL dry toluene at room temperature. The reaction mixture was then left to stir for a further 16 h at 80 °C. The reaction mixture color was turned from yellow to deep brown. The solvent was removed under vacuum, and the residue was extracted through Celite using a CH_2Cl_2/hexane (30:70 v/v) mixture. After evaporation of the solvent, TLC plates were used for chromatographic work-up of the residue. Elution using a mixture of CH_2Cl_2/hexane (30:70 v/v) produced brown solid **3** (0.009 g, 18%; R_f = 0.356). By following similar synthetic strategies, the dark brown solution of *nido*-**2** (0.041 mmol, 0.03 g) in 10 ml dry toluene was charged with $[Co_2(CO)_8]$ (0.082 mmol, 0.028 g) that yielded brown solid **4** (0.012 g, 24%; R_f = 0.363).

3. MS (ESI^+): calcd. for $[C_{28}H_{36}B_6Co_6O_8Se_2+Na]^+$: *m/z* 1100.7246, found: 1100.7235; $^1H\{^{11}B\}$ NMR (500 MHz, $CDCl_3$, 22 °C): δ = 4.53 (br, 1H, B$\underline{H}_t$), 4.15 (br, 1H, B$\underline{H}_t$), 3.65 (s, 2H, B$\underline{H}_t$), 1.77 (s, 30H, $C_5\underline{Me}_5$), -4.42 (2H, Co-$\underline{H}$-B) ppm; $^{11}B\{^1H\}$ NMR (160 MHz, $CDCl_3$, 22 °C, ppm):

δ = 35.6, 30.4, 24.5, 2.6; $^{13}C\{^{1}H\}$ NMR (22 °C, $CDCl_3$, 125 MHz): δ = 99.3 (s, $\underline{C}_5Me_5$), 9.6 (s, $C_5\underline{Me}_5$) ppm; IR (cm^{-1}, CH_2Cl_2): $\bar{\upsilon}$ = 2484 (BH_t), 2083 (CO).

4. MS (ESI^+): calcd. for $[C_{28}H_{36}B_6Co_6O_8Te_2+Na]^+$: *m/z* 1196.7006, found: 1196.6965; $^{1}H\{^{11}B\}$ NMR ($CDCl_3$, 500 MHz, 22 °C): δ = 6.02 (br, 1H, B$\underline{H}_t$), 4.87 (br, 2H, B$\underline{H}_t$), 3.12 (s, 1H, B$\underline{H}_t$), 1.86 (s, 30H, $C_5\underline{Me}_5$), -4.86 (Co-$\underline{H}$-B, 2H) ppm; $^{11}B\{^{1}H\}$ NMR (22 °C, 160 MHz, $CDCl_3$): δ = 38.9, 27.3, 26.6, 8.1 ppm; $^{13}C\{^{1}H\}$ NMR (22 °C, $CDCl_3$, 125 MHz, ppm): δ = 98.8 (s, $\underline{C}_5Me_5$), 10.2 (s, $C_5\underline{Me}_5$); IR (cm^{-1}, CH_2Cl_2): $\bar{\upsilon}$ = 2485 (BH_t), 2000 (CO).

Syntheses of metallaheteroboranes 5 and 6. In a flame-dried Schlenk tube, under an argon atmosphere, a brown solution of **3** (0.020 g, 0.019 mmol) in dry toluene (10 mL) was charged with $[Co_2(CO)_8]$ (0.013 g, 0.038 mmol) at room temperature. The reaction mixture was stirred for further 5 h at RT. The solvent was eliminated under vacuum, and the residue was extracted through Celite using a mixture of CH_2Cl_2/hexane (30:70 v/v). After the solvent evaporation, TLC plates were used for chromatographic work-up of the residue. Elution using a mixture of CH_2Cl_2/hexane (30:70 v/v) produced brown solid **5** (0.004 g, 16%; R_f = 0.214). Under similar reaction conditions, the dark brown solution of **4** (0.017 mmol, 0.020 g) in 10 ml dry toluene was charged with $[Co_2(CO)_8]$ (0.034 mmol, 0.012 g) that yielded brown solid **6** (0.005 g, 21%; R_f = 0.227).

5. MS (ESI^+): calculated for $[C_{32}H_{36}B_6Co_8O_{12}Se_2+H]^+$: *m/z* 1308.5895, found: 1308.5886; $^{1}H\{^{11}B\}$ NMR ($CDCl_3$, 500 MHz, 22 °C): δ = 4.87 (br, 2H, B$\underline{H}_t$), 1.82 (s, 30H, $C_5\underline{Me}_5$), -4.74 (Co-$\underline{H}$-B, 4H) ppm; $^{11}B\{^{1}H\}$ NMR (160 MHz, 22 °C, $CDCl_3$): δ = 24.7, 23.5 ppm; $^{13}C\{^{1}H\}$ NMR ($CDCl_3$, 125 MHz, 22 °C, ppm): δ = 99.3 (s, $\underline{C}_5Me_5$), 9.7 (s, $C_5\underline{Me}_5$); IR (CH_2Cl_2, cm^{-1}): $\bar{\upsilon}$ = 2510 (BH_t), 2018 (CO).

6. MS (ESI^+): calculated for $[C_{32}H_{36}B_6Co_8O_{12}Te_2+H]^+$: *m/z* 1405.5646, found: 1405.5727; $^1H\{^{11}B\}$ NMR (500 MHz, 22 °C, $CDCl_3$,): δ = 3.65 (br, 2H, B$\underline{H}_t$), 1.89 (s, $C_5\underline{Me}_5$, 30H), -5.05 (4H, Co-$\underline{H}$-B) ppm; $^{11}B\{^1H\}$ NMR ($CDCl_3$, 22 °C, 160 MHz,): δ = 27.2 ppm; $^{13}C\{^1H\}$ NMR (125 MHz, 22 °C, $CDCl_3$, ppm): δ = 99.0 (s, $\underline{C}_5Me_5$), 10.1 ($C_5\underline{Me}_5$, s); IR (CH_2Cl_2): $\bar{\upsilon}$ = 2508 (BH_t), 2018 (CO) cm^{-1}.

Synthesis of metallaheteroborane 8. In a moisture-free Schlenk tube, *nido*-**7** (0.030 g, 0.049 mmol) and $[Ru_3(CO)_{12}]$ (0.049 mmol, 0.031 g) were dissolved in toluene (15 ml) at room temperature under an inert atmosphere. Further, the reaction mixture was stirred for 16 h at 80 °C. After solvent removal, the residue was extracted through Celite using a CH_2Cl_2/hexane (20:80 v/v) mixture. After solvent removal, silica gel TLC plates were used to perform a chromatographic work-up. Elution using a CH_2Cl_2/hexane (15:85 v/v) mixture yielded violet solid **8** (0.006 g, 11%; R_f = 0.342).

8. MS (ESI^+): calcd. for $[C_{28}H_{37}B_7Co_2O_8Ru_3Te]^+$: *m/z* 1126.8062, found: 1126.7909. $^1H\{^{11}B\}$ NMR (22 °C, 400 MHz, $CDCl_3$): δ = 1.76 (s, $C_5\underline{Me}_5$, 15H), 1.63 (s, 15H, $C_5\underline{Me}_5$), -8.92 (Ru-$\underline{H}$-B); $^{11}B\{^1H\}$ NMR (22 °C, 160 MHz, $CDCl_3$): δ = 50.0, 39.4, 35.8, 14.9 and 5.6 ppm; $^{13}C\{^1H\}$ NMR ($CDCl_3$, 125 MHz, 22 °C): δ = 98.2, 96.8 ($\underline{C}_5Me_5$, s), 10.1, 9.2 (s, $C_5\underline{Me}_5$) ppm; IR (CH_2Cl_2): $\bar{\upsilon}$ = 2497 (BH_t), 2039, 2005 (CO) cm^{-1}.

Synthesis of metallaheteroborane 10. In a flame-dried Schlenk tube, under an argon atmosphere, *nido*-**9** (0.050 mmol, 0.030 g) and $[Fe_2(CO)_9]$ (0.100 mmol, 0.036 g) were dissolved in 10 ml hexane and then left to stir for 16 h at RT. Under vacuum, the hexane solvent was eliminated and the solid was extracted through Celite using a CH_2Cl_2/hexane (20:80 v/v) mixture. After eliminating solvent, TLC plates were used for chromatographic work-up of the

residue. Elution with a hexane/toluene (70:30 v/v) mixture afforded purple solid *nido*-**10** (0.010 g, 28%; R_f = 0.282).

10. MS (ESI$^+$): calcd. for $[C_{24}H_{36}B_6Co_2FeO_3S_4]^+$: *m/z* 739.0168, found: 739.0144. $^1H\{^{11}B\}$ NMR ($CDCl_3$, 500 MHz, 22 °C): δ = 4.95 (br, B$\underline{H}_t$, 1H), 3.88 (s, 2H, B$\underline{H}_t$), 3.47 (br, 1H, B$\underline{H}_t$), 4.10 (d, 2H, C$\underline{H}_2S_2$), 1.65 (s, Cp*, 30H) ppm; $^{11}B\{^1H\}$ NMR ($CDCl_3$, 160 MHz, 22 °C, ppm): δ = 34.8, 30.7, 26.2, 6.9; $^{13}C\{^1H\}$ NMR ($CDCl_3$, 22 °C, 100 MHz): δ = 98.8 (s, $\underline{C}_5Me_5$), 41.5 (s, $\underline{C}H_2S_2$), 9.1 (s, $C_5\underline{Me}_5$) ppm; IR (CH_2Cl_2): $\bar{\upsilon}$ = 2499 (BH_t), 2055, 2020 (CO) cm^{-1}.

X-ray Structure Analysis: Single-crystals of **3**-**6**, **8**, and **10** were grown by slow diffusion of a solution of CH_2Cl_2-hexane at 5 ˚C. The X-ray data were collected and integrated for **3** and **4** using a Bruker APEX-II CCD, for **5** using Bruker Axs Kappa Apex2 Diffractometer, for **6** using D8 VENTURE Bruker AXS, for **8** using Bruker D8 VENTURE diffractometer with PHOTON II detector and APEXII Bruker-AXS with graphite monochromated Mo-Kα (λ = 0.71073 Å) radiation at 296(2) K (for **3**, **4**, **5**, and **8**), 150(2) K (for **6** and **10**). The structures were solved using SHELXS-97, SHELXT-2014[20] and refined using SHELXL-2014, SHELXL-2017, SHELXL-2018.[21] Olex2 software was used to draw the X-ray structures for all synthesized clusters.[22] Crystallographic data have been deposited with the Cambridge Crystallographic Data Center as supplementary publications CCDC-2160195 (**3**), 2151737 (**4**), 2151736 (**5**), 2144494 (**6**), 2174391 (**8**), and 2151735 (**10**) contain crystallographic data. These data can be obtained free of charge from the Cambridge Crystallographic Data Centre via www.ccdc.cam.ac.uk/data_request/cif.

Crystal data of **3.** $C_{28}H_{36}B_6Co_6O_8Se_2$; formula weight, M_r.= 1076.93; monoclinic; $P2_1/n$; a = 11.9660(7) Å, b = 18.4274(9) Å, c = 16.9432(6) Å, α = 90°, β = 95.015(2)°, γ = 90°; Z = 4; V =

3721.7(3) Å^3; μ = 4.613 mm^{-1}; F(000) = 2112; ρ_{calcd} = 1.922 g/cm^3; R_1 = 0.0415; wR_2 = 0.0783; 5263 independent reflections [2θ ≤ 46.26°], and 469 parameters, Goodness-of-fit on F^2 = 0.987.

Crystal data of **4.** $C_{28}H_{36}B_6Co_6O_8Te_2$, 0.5($C_2Cl_2$); formula weight, M_r.= 1221.67; triclinic; P-1; a = 10.8664(4) Å, b = 12.3963(5) Å, c = 16.9026(8) Å, α = 74.083(2)°, β = 85.568(2)°, γ = 65.494(2)°; Z = 2; V = 1990.57(15) Å^3; μ = 3.990 mm^{-1}; F(000) = 1174; ρ_{calcd} = 2.038 g/cm^3; R_1 = 0.0231; wR_2 = 0.0597; 6975 independent reflections [2θ ≤ 49.99°], and 479 parameters, Goodness-of-fit on F^2 = 1.012.

Crystal data of **5.** $C_{32}H_{36}B_6Co_8O_{12}Se_2$; formula weight, M_r.= 1306.83; orthorhombic; $Fmm2$; a = 19.0340(15) Å, b = 19.3285(17) Å, c = 11.8205(9) Å, α = 90°, β = 90°, γ = 90°; Z = 4; V = 4348.7(6) Å^3; μ = 4.702 mm^{-1}; F(000) = 2552; ρ_{calcd} = 1.996 g/cm^3; R_1 = 0.0399; wR_2 = 0.0869; 2572 independent reflections [2θ ≤ 52.04°], and 155 parameters, Goodness-of-fit on F^2 = 1.067.

Crystal data of **6.** $C_{32}H_{36}B_6Co_8O_{12}Te_2$; formula weight, M_r.= 1404.11; orthorhombic; $Fmm2$; a = 19.067(2) Å, b = 19.096(2) Å, c = 11.6539(13) Å, α =90°, β = 90°, γ = 90°; Z = 4; V = 4243.2(8) Å^3; μ = 4.451 mm^{-1}; F(000) = 2696; ρ_{calcd} = 2.198 g/cm^3; R_1 = 0.0258; wR_2 = 0.0604; 2531 independent reflections [2θ ≤ 54.98°], and parameters 157, Goodness-of-fit on F^2 = 1.197.

Crystal data of **8.** 2($C_{28}H_{37}B_7Co_2O_8Ru_3Te$), CH_2Cl_2; formula weight, M_r.= 2336.75; triclinic; P-1; a = 10.6629(4) Å, b = 11.5666(4) Å, c = 17.9820(7) Å, α = 80.8160(10)°, β = 84.0880(10)°, γ = 64.3040(10)°; V = 1971.42(13) Å^3; μ = 2.783 mm^{-1}; Z = 1; F(000) = 1126; ρ_{calcd} = 1.968 g/cm^3; wR_2 = 0.0962; R_1 = 0.0376; 7312 independent reflections [2θ ≤ 51.00°], and parameters 469, Goodness-of-fit on F^2 = 1.219.

Crystal data of **10.** $C_{24}H_{36}B_6Co_2FeO_3S_4 \cdot CH_2Cl_2$; formula weight, M_r.= 824.26; orthorhombic; *Pnma*; unit cell, a = 17.4175(14) Å, b = 16.4575(12) Å, c = 11.7592(7) Å, α = 90°, β = 90°, γ = 90°; Z = 4; V = 3370.8(4) Å^3; μ = 1.833 mm^{-1}; $F(000)$ = 1680; ρ_{calcd} = 1.624 g/cm^3; wR_2 = 0.1744; R_1 = 0.0833; 3518 independent reflections [2θ ≤ 52.736°], and parameters 149, Goodness-of-fit on F^2 = 1.171.

ASSOCIATED CONTENT

Solid-state X-ray structures; ESI-MS spectra; ^{1}H, ^{1}H{^{11}B}, ^{13}C{^{1}H}, ^{11}B{^{1}H}, HSQC NMR spectra; IR spectra; additional DFT results; and optimized coordinates of synthesized clusters **3-6**, **8**, and **10**.

Supporting Information

The supporting information is available free of charge at website: http://pubs.acs.org.

AUTHOR INFORMATION

Corresponding Author

*E-mail: sghosh@iitm.ac.in (S.G.)

Notes

The authors declare no competing financial interest.

ACKNOWLEDGMENT

This work was supported by SERB, New Delhi, India (grant no. CRG/2019/001280) and the Centre of Excellence on Molecular Materials and Functions under the Institution of Eminence

scheme of IIT Madras. C.N. and K.K. are grateful to DST-INSPIRE, A.R. is grateful to IIT Madras, India for research fellowships. Authors are grateful to Dr. P. K. Sudhadevi Antharjanam and V. Ramkumar for X-ray data analyses. The computational facility of IIT Madras is gratefully acknowledged.

REFERENCES

(1) (a) Lipscomb, W. N. Boron Hydrides, Dover Publications Inc.: Mineola, New York, **2012**. (b) Albert, B; Hillebrecht, H. Boron. Elementary Challenge for Experimenters and theoreticians. *Angew. Chem. Int. Ed.* **2009**, *48*, 8640–8668.

(2) (a) Saha, K.; Roy, D. K.; Dewhurst, R. D.; Ghosh, S.; Braunschweig, H. Recent Advances in the Synthesis and Reactivity of Transition Metal σ-Borane/Borate Complexes. *Acc. Chem. Res*. **2021**, *54*, 1260−1273. (b) Borthakur, R.; Saha, K.; Kar, S.; Ghosh, S. Recent advances in transition metal diborane(6), diborane(4) and diborene(2) chemistry. *Coord. Chem. Rev*. **2019**, *399*, 213021–213037.

(3) (a) Grimes, R. N. *Carboranes*, 3rd ed.; Elsevier, Oxford, UK, 2016, pp 929-944. (b) Zhang, X.; Yan, H. Transition metal-induced B–H functionalization of *o*-carborane. *Coord. Chem. Rev*. **2019**, *378*, 466–482. (c) Kar, S.; Ghosh, S. Borane Polyhedra Beyond Icosahedron. In: Mingos D. (eds) 50th Anniversary of Electron Counting Paradigms for Polyhedral Molecules. In *Structure and Bonding*, Springer, Cham., **2021**, vol. 187.

(4) (a) Hosmane, N. S.; Maguire, J. A. Metallacarboranes of d- and f-Block metals, in: *Comprehensive Organometallic Chemistry III*, Crabtree, R. H.; Mingos, D. M. P.(eds.), Elsevier, Oxford, 2006, vol. 3, ch. 3.05, pp. 175–264. (b) Kar, S.; Pradhan, A. N.; Ghosh, S. Polyhedral Metallaboranes and Metallacarboranes in: *Comprehensive Organometallic Chemistry IV*, 2022.

doi: 10.1016/B978-0-12-820206-7.00169-4. (c) Ghosh, S.; Noll, B. C.; Fehlner, T. P. Borane Mimics of Classic Organometallic Compounds: $[(Cp^*Ru)(B_8H_{14})(RuCp^*)]^{0,+1}$ Isoelectronic Analogues of Dinuclear Pentalene Complexes. *Angew.Chem.Int.Ed.* **2005**, *44*, 6568–6571.

(5) (a) Fehlner, T. P.; Halet, J. -F.; Saillard, J. -Y. *Molecular Clusters: A Bridge to Solid-State Chemistry*, Cambridge University Press: Cambridge, U.K. 2007. (b) Kennedy, J. D. The Polyhedral Metallaboranes Part II. Metallaborane Clusters with Eight Vertices and More. *Prog. Inorg. Chem.* **1986**, *34*, 211−434. (c) Shore, S. G. Studies of the smaller boron hydrides and their derivatives. *Pure Appl. Chem.* **1977**, *49*, 717–732. (d) Yao, Z. -J.; Huo, X. -K.; Jin, G. -X. Zwitterionic half-sandwich Rh and Ir complexes containing a diphosphine *nido*-carborane ligand: synthesis, structure transformation and application in H_2 activation. *Chem. Commun.* **2012**, *48*, 6714–6716. (e) Gao, Y.; Cui, P. -F.; Aznarez, F.; Jin, G. -X. Iridium-Induced Regioselective B-H and C-C Activations at Azo-Substituted *o*-Carboranes. *Chem. Eur. J.* **2018**, *24*, 10357 – 10363.

(6) (a) Pathak, K.; Nandi, C.; Ghosh, S. Metallaheteroboranes with group 16 elements: Aspects of synthesis, framework and reactivity. *Coord. Chem. Rev.* **2022**, *453*, 214303. (b) Nandi, C.; Kar, S.; Zafar, M.; Kar, K.; Roisnel, T.; Dorcet, V.; Ghosh, S. Chemistry of Dimetallaoctaborane(12) with Chalcogen-Based Borate Ligands: Obedient versus Disobedient Clusters. *Inorg. Chem.* **2020**, *59*, 3537-3541. (c) Sahoo, S.; Mobin, S. M.; Ghosh S. Direct Insertion of Sulphur, Selenium and Tellurium atoms into Metallaborane Cages using Chalcogen Powders. *J. Organomet. Chem.* **2010**, *695*, 945-949. (d) Geetharani, K.; Bose, S. K.; Sahoo, S.; Varghese, B.; Mobin, S. M.; Ghosh, S. Cluster Expansion Reactions of Group 6 and 8 Metallaboranes Using Transition Metal Carbonyl Compounds of Groups 7-9. *Inorg. Chem.* **2011**, *50*, 5824-5832. (e) Bose, S. K.; Ghosh, S.; Noll, B. C.; Halet, J. -F.; Saillard, J. -Y.; Vega, A.

Linked and Fused Tungstaborane Clusters: Synthesis, Characterization and Electronic Structures of bis-{(n^5-$C_5Me_5W)_2B_5H_8$}$_2$ and (n^5-$C_5Me_5W)_2${$Fe(CO)_3$}$_n B_{6-n}H_{10-n}$, n = 0,1. *Organometallics* **2007***, 26,* 5377-5385.

(7) Hawthorne, M. F. The Role of Chemistry in the Development of Boron Neutron Capture Therapy of Cancer. *Angew. Chem., Int. Ed. Engl.* **1993**, *32*, 950−984.

(8) Burke, A.; Ellis, D.; Giles,B. T.; Hodson, B. E.; Macgregor, S. A.; Rosair, G. M.; Welch, A. J. Beyond the Icosahedron: The First 13-Vertex Carborane. *Angew. Chem. Int. Ed*. **2003**, *42*, 225−228.

(9) Zheng, F.; Yui, T. H.; Zhang, J.; Xie, Z. Synthesis and X-ray characterization of 15- and 16-vertex *closo*-carboranes. *Nat. Commun.* **2020***, 11,* 5943-5947.

(10) (a) Roy, D. K.; Bose, S. K.; Anju, R. S.; Mondal, B.; Ramkumar, V.; Ghosh, S. Boron Beyond the Icosahedral Barrier: A 16-Vertex Metallaborane. *Angew. Chem. Int. Ed*. **2013**, *52*, 3222–3226. (b) De, A.; Zhang, Q. -F.; Mondal, B.; Cheung, L. F.; Kar, S.; Saha, K.; Varghese, B.; Wang, L. -S.; Ghosh, S. [$(Cp_2M)_2B_9H_{11}$] (M = Zr or Hf): early transition metal 'guarded' heptaborane with strong covalent and electrostatic bonding. *Chem. Sci*. **2018**, *9*, 1976-1981. (c) Ghosh, S.; Fehlner, T. P.; Noll, B. C. Condensed metallaborane clusters: synthesis and structure of $Fe_2(CO)_6$(η^5-C_5Me_5RuCO)(η^5-C_5Me_5Ru)B_6H_{10}. *Chem. Commun*. **2005**, 3080-3082. (d) Bose, S. K.; Geetharani, K.; Varghese, B.; Ghosh, S. Condensed Tantalaborane Clusters: Synthesis and Structures of [$(Cp^*Ta)_2B_5H_7${$Fe(CO)_3$}$_2$] and [$(Cp^*Ta)_2B_5H_9${$Fe(CO)_3$}$_4$]. *Inorg. Chem.* **2011**, *50*, 2445–2449. (e) Dhayal, R. S.; Sahoo, S.; Reddy, K. H. K.; Mobin, S. M.; Jemmis, E. D.; Ghosh, S. Vertex-Fused Metallaborane Clusters: Synthesis, Characterization and Electronic Structure of [(n^5-$C_5Me_5Mo)_3MoB_9H_{18}$]. *Inorg. Chem.* **2010**, *49*, 900–904.

(11) Ghosh, S.; Noll, B. C.; Fehlner, T. P. Expansion of iridaborane clusters by addition of monoborane. Novel metallaboranes and mechanistic detail. *Dalton Trans.* **2008**, 371–378.

(12) (a) Wade, K. Skeletal electron counting in cluster species. Some generalisations and predictions. *Inorg. Nucl. Chem. Lett*. **1972**, *8*, 559-562. (b) Mingos, D. M. P.; Wales, D. J. *Introduction to Cluster Chemistry*, Prentice Hall, New York, **1990**. (c) Jemmis, E. D.; Balakrishnarajan, M. M.; Pancharatna, P. D. A Unifying Electron-Counting Rule for Macropolyhedral Boranes, Metallaboranes, and Metallocenes. *J. Am. Chem. Soc.* **2001**, *123*, 4313–4323.

(13) Hoffmann, R. Building Bridges Between Inorganic and Organic Chemistry (Nobel Lecture). *Angew. Chem. Int. Ed. Engl*. **1982**, *21*, 711-724.

(14) Zafar, M.; Kar, S.; Nandi, C.; Ramalakshmi, R.; Ghosh, S. Cluster Fusion: Face-fused Macropolyhedral Tetracobaltaboranes. *Inorg. Chem*. **2019**, 58, 47-51.

(15) Kaur, P.; Thornton-Pett, M.; Clegg, W.; Kennedy, J. D. Macropolyhedral boron-containing cluster chemistry: nineteen-vertex $[(PPh_3)NiS_2B_{16}H_{12}(PPh_3)]$ and eighteen-vertex $S_2B_{16}H_{14}(PPh_3)$, *J. Chem. Soc. Dalton Trans.* **1996**, *1996*, 4155–4157.

(16) Barton, L.; Bould, J.; Kennedy, J. D.; Rath, N. P. Macropolyhedral boron-containing cluster chemistry. Isolation and characterisation of the eighteen-vertex nido-5′-iridaoctaborano [3′,8′:1′,2]-closo-4-iridadodec aborane, $[(CO)(PMe_3)_2IrB_{16}H_{14}Ir(CO)(PMe_3)_2]$. *J. Chem. Soc.*, *Dalton Trans.* **1996**, 3145−3149.

(17) di Biani, F. F.; Laschi, F.; Zanello, P.; Ferguson, G.; Trotter, J.; O'Riordand, G. M.; Spalding, T. R. Synthesis, structure, spectroscopic and electrochemical study of the paramagnetic

compound [2-(η^7-C_7H_7)-7,11-F_2-2,1-closo-$MoTeB_{10}H_8$]. *J. Chem. Soc., Dalton Trans.* **2001**, 1520-1523.

(18) Joseph, B.; Barik, S. K.; Ramalakshmi, R.; Kundu, G.; Roisnel, T.; Dorcet, V.; Ghosh, S. Chemistry of Triple-Decker Sandwich Complexes Containing Four-Membered Open B_2E_2 Rings (E = S or Se). *Eur. J. Inorg. Chem*. **2018**, 2045–2053.

(19) Nandi, C.; Kar, K. Gayen, S. Roisnel, T. Ghosh S. Directed Syntheses of CS_2- and CS_3-Bridged Decaborane-14 Analogues. *Inorg. Chem*. **2021,** *60*, 12367−12376.

(20) (a) Sheldrick, G. M. SHELXT - Integrated space-group and crystal-structure determination. *Acta Cryst.* **2015**, *A71*, 3–8. (b) Sheldrick, G. M. SHELXS97 and SHELXL97. Program for Crystal Structure Solution and Refinement, University of Gottingen: Germany, 1997.

(21) Sheldrick, G. M. SHELXT – Crystal structure refinement with SHELXL. *Acta Cryst.* **2015**, *C71*, 3–8.

(22) Dolomanov, O. V.; Bourhis, L. J.; Gildea, R. J.; Howard, J. A. K.; Puschmann, H. OLEX2: a complete structure solution, refinement and analysis program. *J. Appl. Crystallogr.* **2009**, *42*, 339–341.

For Table of Contents Only

Cluster Growth Reactions: Structures and Bonding of Metal-Rich Metallaheteroboranes Containing Heavier Chalcogen Elements

Chandan Nandi,[a] Arindam Roy,[a] Ketaki Kar,[a] Marie Cordier[b] and Sundargopal Ghosh[*,a]*

Cluster expansion reactions of 10-vertex decaborane(14) analogs with various metal carbonyls. Unusual 13- and 14-vertex face-fused and 16-vertex doubly-face-fused polyhedral clusters (see pictures).